SnT 2019
CTBT: SCIENCE AND TECHNOLOGY CONFERENCE

Properties of the high-frequency ambient seismic field recorded on a large-N (N=10,530) seismic deployment in the Vienna Basin

S. Schippkus [1, c], M. Garden [2], G. Bokelmann [1]

[c]ontact: *sven.schippkus@univie.ac.at*
[1] Department for Meteorology and Geophysics, University of Vienna, Vienna, Austria
[2] OMV, Geophysics, Vienna, Austria

T1.2 - P71

Introduction

The Vienna Basin is the largest petroleum basin in Austria. As part of the ongoing seismic exploration for hydrocarbon resources in the basin, a large-N (N=10,530) dataset of continuous seismic recordings of the ambient seismic field was acquired in early 2018. Data were recorded on geophones (10-Hz corner frequency) and each location was made up of 12 or 24 densely clustered geophones, which were stacked to increase signal-to-noise ratio. Data were collected by these geophone clusters for up to 6 days, recorded only during day time. The station locations are distributed on a grid of roughly 40m by 400m and cover an area of about 500km² (**Figure 1**).

We are in the process of imaging the upper part (top few kilometers) of the Vienna Basin by surface-wave tomography using surfaces waves extracted from ambient noise. For this, we study the properties of the ambient seismic field to ensure that the ambient seismic field contains surface waves that are appropriate for our purposes.

Here, we present the first insights into the ambient seismic field in the Vienna Basin retrieved from this dataset.

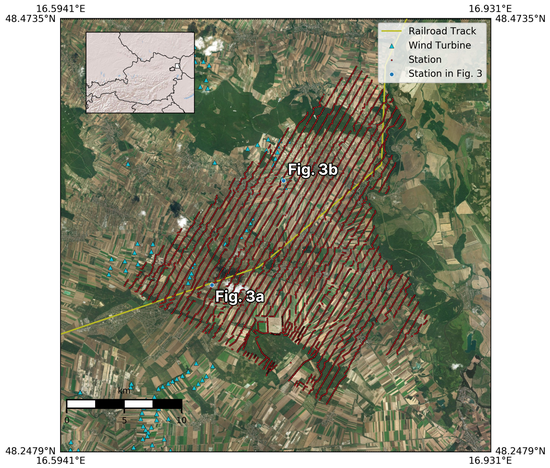

Figure 1

Map of study area with distribution of stations, and expected local noise sources (railroad track, wind turbines).

Noise Levels

The mean absolute amplitudes for each station, measured on unfiltered data (**Figure 2**), reveal human activity and local noise sources remarkably well. Trains, cars, town centers, and wind parks are all well-visible in the map view. The animated movie (1min per frame) reveals daily activity with remarkable clarity.

Noteworthy Signals

While this study is focussed on the ambient seismic field, this unique data set allows observation of several interesting signals. These include signals of trains and cars (**Figure 3a**, *Fuchs et al., 2017*), spectral lines induced by the power network (**Figure 3a**), airplanes passing by the network (**Figure 3b**, *Meng and Ben-Zion, 2018*), and spectral lines induced by a nearby wind turbine (**Figure 3b**).

Figure 2

Map of mean absolute amplitudes for all 10530 stations. High amplitudes are found where expected noise sources are nearby.

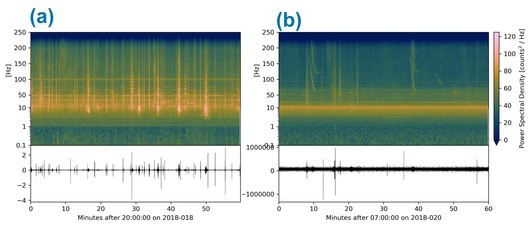

Figure 3

Raw seismic records (bottom panels) and spectrograms (top panels) of 1-hour windows recorded at different stations and different times. Signals of trains and the power network (**a**), airplanes passing by the network (**b**), and wind turbines (**b**).

Animations will be on display during attendance time.

Beamforming

We perform beamforming on 50 subarrays (of 6 stations each) distributed evenly throughout the network (**Figure 4**). We use overlapping 1min-windows and find coherent signals in the frequency range of 0.1–0.5Hz, exceeding our expections of the 10Hz geophones. These signals arrive from NW (~300°) with velocities of ~2–4km/s, consistent with Rayleigh waves, generated in the oceans (*Juretzek and Hadziioannou, 2016*).

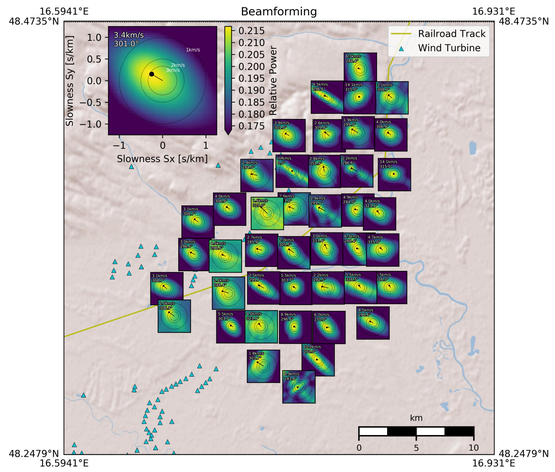

Figure 4

Beamforming results for 0.1–0.5Hz. **Top left panel**: Mean relative power map of all subarrays. **Other panels**: Relative power maps for subarrays analogue to top left panel.

Cross-Correlations

Cross-correlation functions (CCFs) of ambient noise are computed with a processing scheme closely following *Schippkus et al., 2018.*

One example virtual source is shown in **Figure 5**. When sorted and binned by distance to the virtual source (bottom left panel), the normalized CCFs contain clear wave trains on the acausal and causal parts of the CCF in frequencies from 0.2 – 2Hz (*up to ~10Hz, not shown here*).

Animated movies of the CCFs with time reveal that the wavefield is more complex than the binned CCFs suggest. Depending on the frequency band, the wavefield contains different features.

We classify these features into five categories: **MS, SS, ↘, ↗, 0** (**Table 1**). They are observed consistently for 20 virtual sources distributed evenly throughout the network.

Using only data from 23rd Jan., the influence of **SS** is mitigated (**Figure 6**), as the local wind park is mostly inactive on that day (see **Figure 2**).

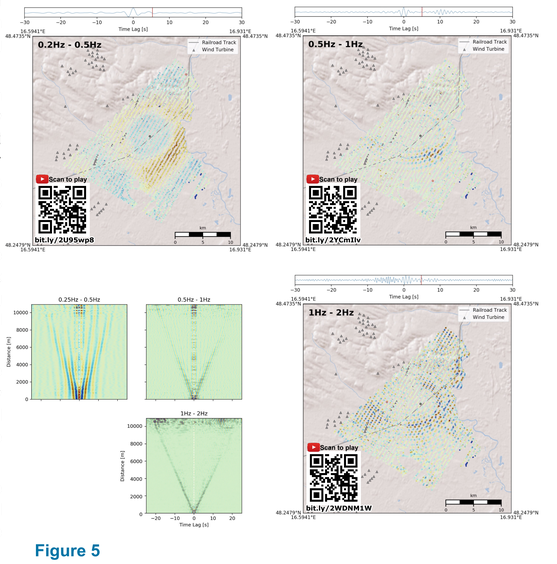

Figure 5

Spatial distribution of CCFs for a station near the center (FAJB), filtered in three frequency bands (0.2–0.5Hz, 0.5–1Hz, 1–2Hz). **Bottom Left**: Correlation vs. distance plots. **Other panels**: Snapshots of the CCFs in a map view.

0.2 – 0.5Hz	MS	SS	↘	↗	0
AGCD	x	o	o	o	~
AJMI	x	o	x	o	~
BBFH	x	o	x	o	o
BDGI	x	o	o	o	~
BFFJ	x	o	x	o	o
BIFJ	x	o	~	o	x
CAAD	x	o	~	o	x
CFKF	x	o	~	o	~
CJJE	x	o	~	o	x
DHCA	~	o	~	o	x
DIAB	x	o	x	o	~
DKDB	x	o	x	o	~
DKHI	x	o	~	o	~
EGAG	x	o	x	o	~
FAJB	x	o	x	o	x
FDDA	x	o	x	o	x
GBKJ	x	o	~	o	x
GKKJ	x	o	~	o	x
HHAA	x	o	x	o	~
HIGH	x	o	x	o	~
HKAD	x	o	o	o	x

0.5 – 1Hz	MS	SS	↘	↗	0
AGCD	~	x	o	o	x
AJMI	x	x	o	o	x
BBFH	x	x	o	o	o
BDGI	x	x	o	o	~
BFFJ	x	x	o	o	o
BIFJ	~	o	o	o	x
CAAD	x	x	o	o	o
CFKF	x	x	o	o	~
CJJE	o	x	o	o	x
DHCA	x	o	o	o	x
DIAB	x	x	o	o	~
DKDB	x	x	o	o	~
DKHI	~	o	~	o	~
EGAG	x	~	o	o	x
FAJB	x	x	o	o	x
FDDA	x	o	o	o	~
GBKJ	x	o	o	o	x
GKKJ	x	~	o	o	x
HHAA	x	~	o	o	x
HIGH	x	o	o	o	x
HKAD	x	o	o	o	x

1 – 2 Hz	MS	SS	↘	↗	0
AGCD	o	x	o	x	~
AJMI	~	x	o	o	x
BBFH	x	x	o	o	o
BDGI	x	x	o	~	x
BFFJ	o	x	o	o	o
BIFJ	o	x	o	x	x
CAAD	~	x	o	x	o
CFKF	~	x	o	o	~
CJJE	o	x	o	x	x
DHCA	~	x	o	o	o
DIAB	x	x	o	o	~
DKDB	~	o	o	o	~
DKHI	~	~	o	~	~
EGAG	x	x	o	x	o
FAJB	~	x	o	x	o
FDDA	~	x	o	o	o
GBKJ	x	x	o	x	~
GKKJ	~	x	o	o	x
HHAA	x	~	o	o	o
HIGH	x	~	o	o	o
HKAD	x	x	o	x	x

Table 1

Observation of wavefield features in CCFs at 20 virtual sources.

Legend

MS : Main source
SS : Secondary source
↘ : Plane wave from NW
↗ : Plane wave from SW
0 : Near-0 arrivals

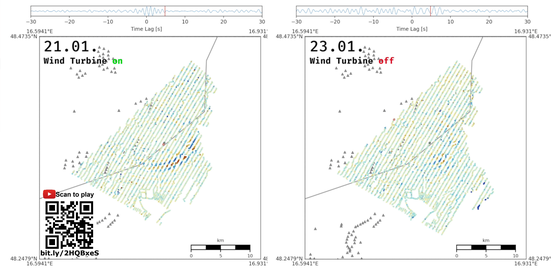

Figure 6

Comparison of CCFs computed from data recorded on Sunday, 21st Jan (left) vs. Tuesday, 23rd Jan (right). Clear mitigation of the wavefield originating from the secondary source.

Conclusions

The ambient seismic field recorded in an area of significant human activity is dominated by cultural noise sources at frequencies higher than ~1Hz, e.g., trains, cars, wind turbines (**Figure 2, 3**). At frequencies near the microseism peak (~0.25Hz) we find the noise to be preferentially coming from NW (**Figure 4**), suggesting that we may utilize microseisms to image the underground even on this installation of 10Hz geophones.

The CCFs show several noteworthy features (**Figure 5, Table 1**), e.g., a strong secondary source, and strong near-0 arrivals. Wind turbines are stationary sources that emit seismic waves continuously over long periods of time and thus can introduce 'secondary wavefields' in the CCFs. We are able to image these thanks to the dense station spacing (**Figure 5**), and note that they may get concealed when looking at distance-binned CCFs (**Figure 5**). These wavefields can be mitigated by using data with low wind turbine activity (**Figure 6**).

References

Juretzek, C. & Hadziioannou, C. (2016) **Where do ocean microseisms come from? A study of Love-to-Rayleigh wave ratios**. J. Geophys. Res. Solid Earth, 121, 6741–6756. doi:10.1002/2016JB013017

Schippkus, S., Zigone, D., Bokelmann, G.the AlpArray Working Group. (2018) **Ambient-noise tomography of the wider Vienna Basin region**. Geophys. J. Int., 215, 102–117, Oxford University Press. doi:10.1093/gji/ggy259